SLAC–PUB–7729
August 1997

HEAVY FLAVOR PHYSICS AT SLD*

K. Baird, for the SLD Collaboration
Department of Physics and Astronomy, University of Massachusetts,
Amherst, Massachusetts 01003

Abstract

This talk reviews recent results for nine different measurements on various aspects of heavy hadron production, mixing, and decay. The analyses are based upon the data collected using the SLC Large Detector (SLD) at the SLAC Linear Collider (SLC). The combination of highly polarized electron beams, small and stable beam spots, and the CCD vertex detector of the SLD allow for many unique and precise measurements.

Invited talk presented at the 25th SLAC Summer Institute on Particle Physics: Physics of Leptons (SSI 97)

Stanford, California

4-15 August 1997

* Work supported in part by Department of Energy contract DE–AC03–76SF00515.

HEAVY FLAVOR PHYSICS AT SLD

Ken Baird*
Department of Physics and Astronomy
University of Massachusetts, Amherst, MA 01003

Representing the SLD Collaboration

ABSTRACT

This talk reviews recent results for nine different measurements on various aspects of heavy hadron production, mixing, and decay. The analyses are based upon the data collected using the SLC Large Detector (SLD) at the SLAC Linear Collider (SLC). The combination of highly polarized electron beams, small and stable beam spots, and the CCD vertex detector of the SLD allow for many unique and precise measurements.

*Work supported in part by DOE Contracts DE-FG02-92ER40715 (Massachusetts) and DE-AC03-76SF00515 (SLAC).

1 Introduction

The measurements discussed herein are based upon the e^+e^- annihilation data collected by the SLC Large Detector (SLD). With two exceptions (discussed in Secs. 7 and 13), all of the measurements use the 150,000 hadronic Z^0 decays collected in the 1993 and 1994–95 physics runs.

This paper is organized as follows: Secs. 2, 3, and 4 describe the accelerator and detector, the techniques used to select B hadrons, and the tools used to tag the flavor of the B at the time of production. Sections 5 through 12 discuss specific measurements, outlining the motivation, procedures, and results. Finally, a brief summary is given in Sec. 13.

2 The SLC and SLD

At the SLAC Linear Collider (SLC), shown in Fig. 1, polarized electrons[1] are photoemitted from a strained lattice GaAs photocathode. The spin vector of these electrons is rotated so that it is vertical during the damping and acceleration phases. At the end of the linac, the polarization axis is rotated by a series of betatron oscillations so that it is longitudinal at the interaction point. These longitudinally polarized electrons are annihilated with unpolarized positrons at the Z^0 resonance, and are recorded using the SLD Experiment.[2] A quadrant view of the SLD is shown in Fig. 2. As is discussed below, the tightly focused and very stable beam spots allow for precise interaction point determination.

In the SLD, charged tracks are measured using the vertex detector (VXD, discussed below) and the Central Drift Chamber (CDC). Momentum measurement is provided by a uniform axial magnetic field of 0.6 T. Particle identification is performed using the Cherenkov Ring-Imaging Detector (CRID, discussed below). Particle energy measurements and electron identification are performed using the Liquid Argon Calorimeter (LAC). Muon identification is performed using the Warm Iron Calorimeter (WIC).

2.1 The SLD Vertex Detectors

For the 1992–1995 physics runs, the SLD utilized a novel high-resolution CCD vertex detector referred to herein as VXD2 (Ref. 3). This device provides true

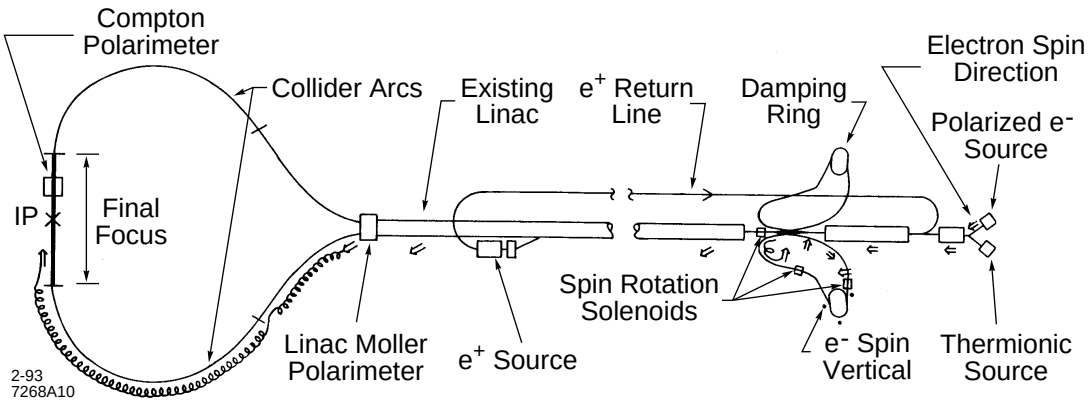

Figure 1: A schematic view of the SLAC Linear Collider (SLC).

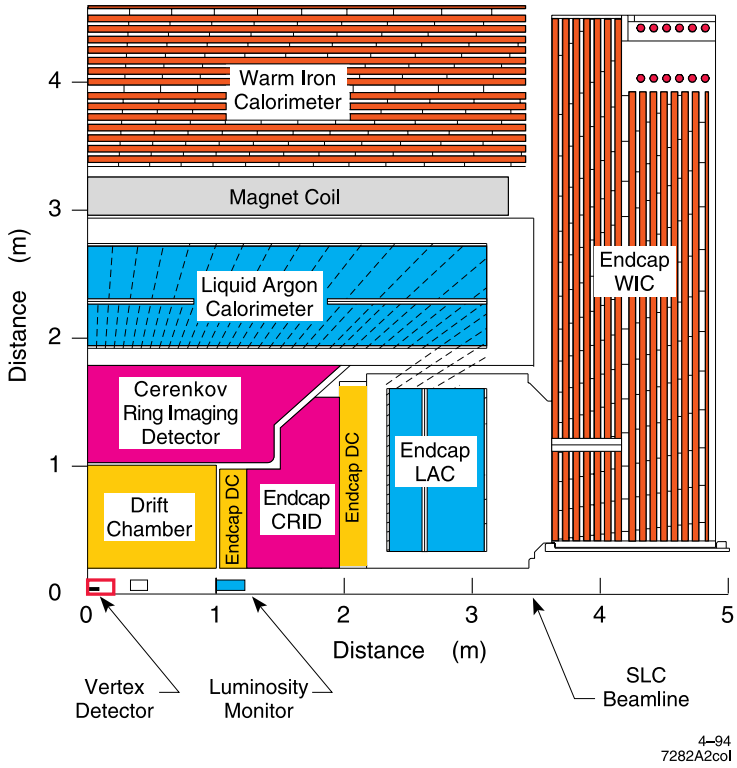

Figure 2: A quadrant view of the SLD detector.

three-dimensional information and a single hit resolution of 5.6 μm in the $r\phi$ plane (transverse to the beam axis) and 6.2 μm in the rz plane (containing the beam axis). The inner VXD2 radius is 2.95 cm and there is a minimum of two hits per track within $|\cos\theta| < 0.74$—the average number of hits is 2.3. The combined impact parameter resolution (CDC + VXD2) at high momentum was determined from $Z^0 \to \mu^+\mu^-$ decays to be $\sigma(r\phi) = 11$ μm and $\sigma(rz) = 37$ μm. Multiple scattering yielded an additional momentum-dependent contribution parameterized as $\sigma = 70\ \mu\text{m}/(p\ \sin^{3/2}\theta)$, where the momentum p is expressed in GeV/c.

The transverse position of the IP is determined using samples of ~ 30 consecutive hadronic Z^0 decays with an accuracy of $7 \pm 2\ \mu$m. The longitudinal IP position is determined on an event-by-event basis with an accuracy of $32\,\mu$m for Z^0 decays into light-flavor quarks (uds), $36\,\mu$m for $Z^0 \to c\bar{c}$ decays, and $52\,\mu$m for $Z^0 \to b\bar{b}$ decays, as determined from the Monte Carlo (MC).

Prior to the 1996 physics run, an upgraded CCD vertex detector (VXD3) was installed.[4] This new device, thus far utilized in only one of the analyses presented below, makes several improvements over VXD2:

- The angular coverage is increased with maximum $|\cos\theta|$ of 0.90 instead of 0.74 for tracks with two hits.
- The average number of hits per track is increased from 2.3 to 3.2.
- The amount of material is reduced from 1.15% to 0.40% of a radiation length per CCD "ladder."
- The average distance between the inner and outer layer is increased from 12 to 20 mm to provide an increased lever-arm.

These features lead to significant improvements in resolution. In particular, the decay length resolution improves roughly by a factor of two.

2.2 The SLD Cherenkov Detector

Another (almost) unique feature of the SLD is the Cherenkov Ring Imaging Detector[5] (CRID) which allows charged particle identification over most of the momentum range. The CRID contains both a liquid radiator and a gas radiator system (see Fig. 3).

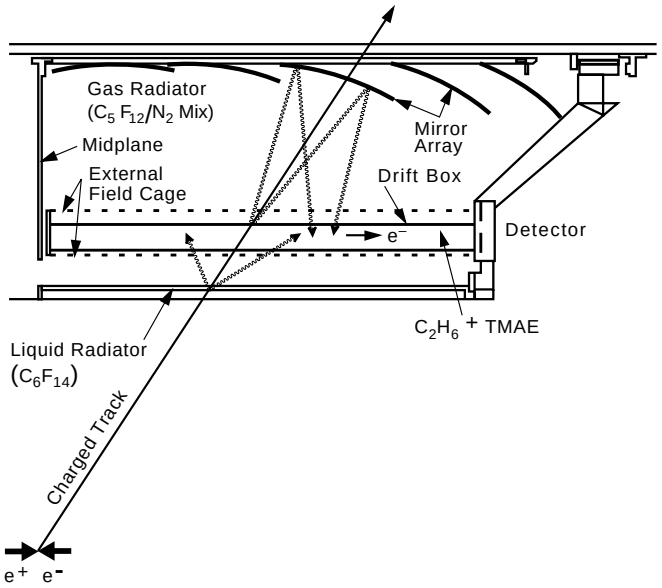

Figure 3: Cross-section view of one CRID quadrant.

The liquid radiator provides low momentum identification with π/K (K/p) separation up to ~ 4 GeV/c (~ 8 GeV/c), whereas the gas radiator provides π/K (K/p) separation above ~ 2.5 GeV/c (~ 9 GeV/c).

3 Heavy Quark Event Tagging

For the analyses described below, three different techniques are used to select high-purity $Z^0 \to b\bar{b}$ events. One technique is to reconstruct a $D^{(*)}$ candidate from three or more charged tracks, and attach it to an identified lepton. This technique is used for the measurement of the b-quark fragmentation function (Sec. 5), one of the two B meson lifetime measurements (Sec. 7), and for one of the four B_d^0 mixing measurements discussed in Sec. 12.1.

A more common technique is to use an impact-parameter (or "lifetime") tag. For this technique, tagging is performed by counting the number of well-measured tracks that are inconsistent with originating from the interaction point (IP). Tracks are considered to be inconsistent if their two-dimensional impact parameter, with respect to the IP, is greater than 3σ. Figure 4 illustrates the use of this technique for the particle production analysis discussed in Sec. 7. Events with no "significantly separated" tracks ($n_{sig} = 0$) are tagged as "uds" events (i.e., $Z^0 \to u\bar{u}, d\bar{d}, s\bar{s}$) and are $\sim 85\%$ pure. Events with $n_{sig} \geq 3$ are tagged as

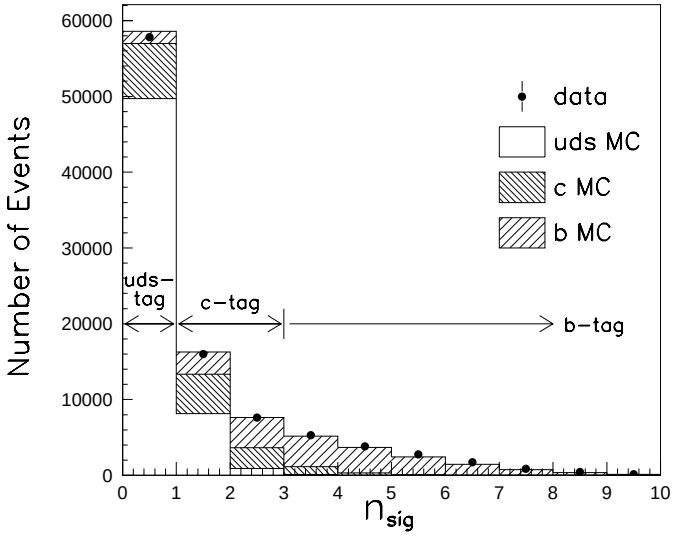

Figure 4: A typical n_{sig} distribution.

$Z^0 \to b\bar{b}$ events and are $\sim 89\%$ pure. The remaining events are tagged as $Z^0 \to c\bar{c}$ events, and are $\sim 33\%$ pure. Note that this flavor tag procedure is 100% efficient; an event is always tagged as either a "*uds*," "$c\bar{c}$," or "$b\bar{b}$" event.

The most common technique used in the analyses below is a unique "topological vertex" tag. This technique utilizes the fine resolution of the SLD vertex detector to reconstruct the B decay vertex for multi-track decays.

The topological vertex reconstruction is applied separately to the tracks in each hemisphere (defined with respect to the event thrust axis). The vertexing algorithm is described in detail in Ref. 6. The vertices are reconstructed in three-dimensional coordinate space by defining a vertex function $V(\mathbf{r})$ at each position $\mathbf{r}$. The helix parameters for each track i are used to describe the three-dimensional track trajectory as a Gaussian tube $f_i(\mathbf{r})$, where the width of the tube is the uncertainty in the measured track location close to the IP. A function $f_0(\mathbf{r})$ is used to describe the location and uncertainty of the IP. $V(\mathbf{r})$ is defined as a function of $f_0(\mathbf{r})$ and the $f_i(\mathbf{r})$ such that it is small in regions where fewer than two tracks (required for a vertex) have significant $f_i(\mathbf{r})$, and large in regions of high track multiplicity. Maxima are found in $V(\mathbf{r})$ and clustered into resolved spatial regions. Tracks are associated with these regions to form a set of topological vertices. For hemispheres containing more than one secondary vertex, the "seed" vertex is chosen to be the one with the highest $V(\mathbf{r})$ value. Vertices consistent

with $K_s^0 \to \pi^+\pi^-$ decays are excluded from the seed vertex selection and the two tracks are discarded.

A vertex axis is formed by a straight line joining the IP to the seed vertex. An algorithm is used to attach secondary tracks to this seed vertex based upon the point of closest approach, and distance of closest approach, to this axis. This set of tracks attached to the seed vertex is fitted to a common vertex.

The mass M of the reconstructed vertex is calculated by assuming each track has the mass of a pion. The transverse component p_T of the total momentum of vertex tracks relative to the vertex axis is calculated in order to determine the p_T corrected mass:

$$M_{P_T} = \sqrt{M^2 + p_T^2} + |p_T|. \tag{1}$$

This quantity is the minimum mass the decaying hadron could have in order to produce a vertex with the quantities M and p_T. The direction of the vertex axis is varied within the 1σ limits constraining the axis at the measured IP and reconstructed seed vertex such that the p_T is minimized within this variation.

A comparison of the reconstructed vertex and the p_T-corrected mass M_{P_T} between data and Monte Carlo is shown in Fig. 5. This figure shows that a large fraction of the charm and light flavor contamination in the sample is eliminated by requiring $M_{P_T} > 2$ GeV/c^2. Using M_{p_T} cuts, b hemispheres can be selected with a purity of $\sim 98\%$.

4 Initial State Tagging

For several of the analyses discussed below, it is necessary to tag the initial state flavor of the B hemisphere as originating from a b-quark or a $\bar{b}$-quark. Two techniques are used: (i) the polarized forward-backward asymmetry, and (ii) the momentum-weighted "jet charge" of the opposite hemisphere.

By assuming the parity-violating nature of the weak interaction (SLD's precision tests of this are discussed in the talk by B. Schumm[7]), the polarized electron beam produced by the SLC can be utilized to tag a hemisphere as originating from a b or $\bar{b}$ quark. As is shown in Fig. 6, outgoing quarks tend to go in the same direction as incident left-handed fermions. The purity of the tag is dependent upon the polar angle of the outgoing quark. By approximating the quark

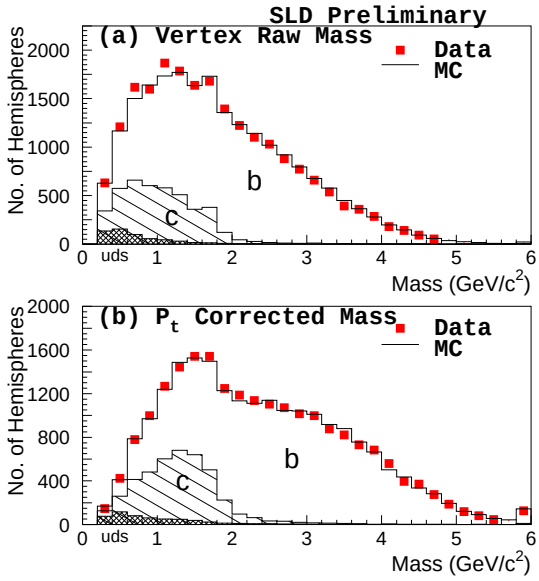

Figure 5: A comparison of data to MC for (a) the raw vertex mass, and (b) the p_T corrected mass (VXD2).

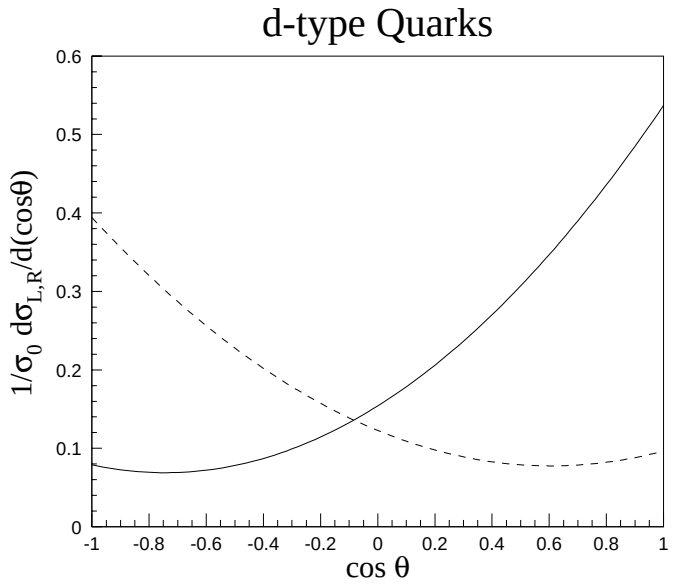

Figure 6: The Electroweak Production Asymmetry for down-type (d, s, b) quarks as a function of the angle between the incident electron beam and the outgoing quark. The solid line is for left-handed electrons, and the dashed line is for right-handed electrons. In both cases, $|P_e| = 73\%$.

direction by the thrust axis of the hemisphere, this angular distribution may be used to calculate the tag purity.

The polarized forward-backward asymmetry $A_{FB}(P_e, \cos\theta)$ can be described by

$$A_{FB}(P_e, \cos\theta) = 2A_b \, \frac{A_e - P_e}{1 - A_e P_e} \, \frac{\cos\theta}{1 + \cos^2\theta} \ , \tag{2}$$

where $A_b = 0.935$ and $A_e = 0.155$ (Standard Model values), P_e is the electron beam longitudinal polarization, and θ is the angle between the thrust axis and the electron beam direction (the thrust axis is signed such that it points in the same hemisphere as the reconstructed vertex). The probability for correctly tagging a b quark at production using the e^- beam polarization is expressed as

$$P_A(b) = \frac{1 + A_{FB}(P_e, \cos\theta)}{2} \ . \tag{3}$$

For $|P_e| = 77\%$, the average purity of this tag is $\sim 72\%$ with 100% efficiency.

A jet charge technique is used in addition to the polarized forward-backward asymmetry. For this tag, tracks in the hemisphere *opposite* that of the reconstructed vertex are selected. These tracks are required to pass quality requirements such as minimum p_T, maximum cosine of the polar angle, etc. With these tracks, an opposite hemisphere momentum-weighted track charge is defined as

$$Q_{opp} = \sum_i q_i \left| \vec{p}_i \cdot \hat{T} \right|^{\kappa} \ , \tag{4}$$

where q_i is the electric charge of track i, $\vec{p}_i$ its momentum vector, $\hat{T}$ is the thrust axis direction, and κ is a coefficient chosen to be 0.5 to maximize the separation between b and $\overline{b}$ quarks. The probability for correctly tagging a b quark in the initial state of the vertex hemisphere can be parameterized as

$$P_Q(b) = \frac{1}{1 + e^{\alpha Q_{opp}}} \ , \tag{5}$$

where the coefficient α is determined using the Monte Carlo simulation. This technique is independent of the polarized forward-backward asymmetry tag. The average purity of the b tag is typically $\sim 67\%$ for this technique. Once again, the efficiency of the tag is 100%.

These two initial state tags can be combined to form an overall initial state tag with b quark probability $P_i(b)$ (a function of P_e, $\cos\theta$, and Q_{opp}):

$$P_i(b) = \frac{P_A(b)P_Q(b)}{P_A(b)P_Q(b) + (1-P_A(b))(1-P_Q(b))}. \quad (6)$$

When combined, the average purity of the b tag is $\sim 82\%$ with 100% efficiency.

5 A Measurement of the b Quark Fragmentation Function

The production of heavy hadrons (H) in e^+e^- annihilation provides a laboratory for the study of heavy-quark (Q) jet fragmentation. This is commonly characterized in terms of the observable $x_{E_H} \equiv 2E_H/\sqrt{s}$, where E_H is the energy of a B or D hadron containing a b or c quark, respectively, and $\sqrt{s}$ is the c.m. energy. In contrast to light-quark jet fragmentation, one expects[8] the distribution of x_{E_H}, $D(x_{E_H})$, to peak at an x_{E_H} value significantly above zero. Since the hadronization process is intrinsically non-perturbative, $D(x_{E_H})$ cannot be calculated directly using perturbative Quantum Chromodynamics (QCD). However, the distribution of the closely-related variable $x_{E_Q} \equiv 2E_Q/\sqrt{s}$ can be calculated perturbatively[9–11] and related, via model-dependent assumptions, to the observable quantity $D(x_{E_H})$; a number of such models of heavy quark fragmentation have been proposed.[12–14] Measurements of $D(x_{E_H})$ thus serve to constrain both perturbative QCD and the model predictions. Furthermore, the measurement of $D(x_{E_H})$ at different c.m. energies can be used to test QCD evolution, and comparison of $D(x_{E_B})$ with $D(x_{E_D})$ can be used to test heavy quark symmetry.[15] Finally, the uncertainty on the forms of $D(x_{E_D})$ and $D(x_{E_B})$ must be taken into account in studies of the production and decay of heavy quarks (see Ref. 16); more accurate measurements of these forms will allow increased precision in tests of the electroweak heavy-quark sector.

Here we consider measurement of the B hadron scaled energy distribution $D(x_{E_B})$ in Z^0 decays. Earlier studies[17] used the momentum spectrum of the lepton from semi-leptonic B decays to constrain the mean value $< x_{E_B} >$ and found it to be approximately 0.70; this is in agreement with the results of similar studies at $\sqrt{s} = 29$ and 35 GeV (Ref. 18). In more recent analyses[19,20] the scaled energy distribution $D(x_{E_B})$ has been measured by reconstructing B hadrons via

their $B \to DlX$ decay mode; we have applied a similar technique. We used the precise SLD tracking system to select jets containing a $B \to DlX$ decay, where the charmed hadron D was identified semi-inclusively from a secondary decay vertex formed from charged tracks. Each hadronic vertex was then associated with a lepton l ($l = e$ or μ) with large momentum transverse to the jet direction.

The final sample comprises 597 events, 293 in the muon channel and 304 in the electron channel. Using the simulation, we estimate that the purity of this sample, defined to be the fraction of the tagged events whose identified leptons l are from true $B \to DlX$ decays, is 69.2%; a further 18% of the selected events contain B decays with a cascade, punch-through, or misidentified lepton, and are still useful. The remaining 12.8% of the event sample comprises non-$b\bar{b}$ events. The efficiency for selecting B hadron decays in the selected hadronic event sample is shown, as a function of x_{E_B}, in Fig. 7; the overall efficiency is 1.1%.

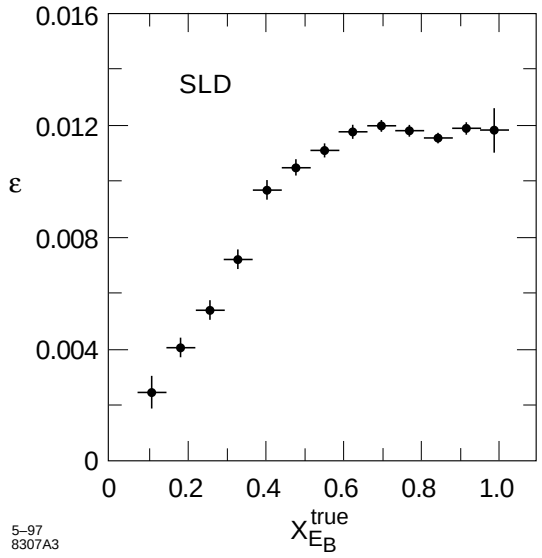

Figure 7: The efficiency ϵ for selecting B hadron decays, as a function of scaled energy x_{E_B}. Note that the first bin (no point shown) is beneath the kinematic limit for x_{E_B}.

Neutral energy depositions measured in the hermetic LAC calorimeter, as well as the energies of charged tracks that were not associated with the Dl system, were subtracted from the jet energy to yield the reconstructed B hadron energy. The final corrected distribution of scaled B hadron energies is shown in Fig. 8.

It is conventional to evaluate the mean of this distribution, $< x_{E_B} >$. Combining all systematic errors in quadrature we obtain:

$$< x_{E_B} > \;\; = \;\; 0.716 \pm 0.011(stat.)^{+0.021}_{-0.022}(syst.).$$

Further details of this analysis may be found in Ref. 21.

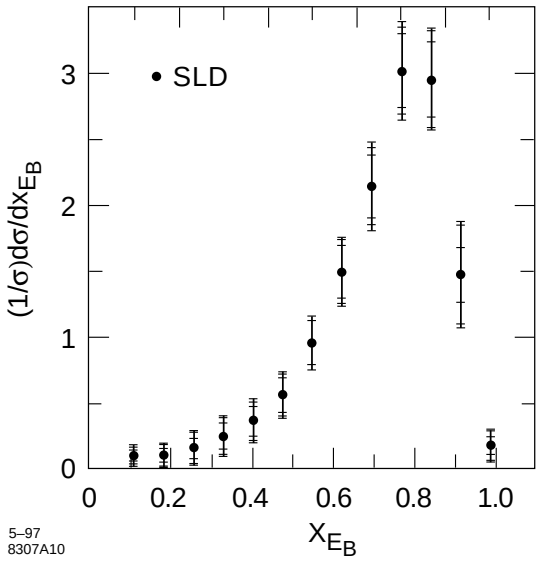

Figure 8: The final corrected distribution of scaled B hadron energies. In each bin the statistical error is indicated by the innermost error bar; the quadrature sum of statistical and experimental systematic errors by the middle error bar; and the quadrature sum of statistical, experimental systematic, and unfolding errors by the outermost error bar. Note that the first bin (no point shown) is beneath the kinematic limit for x_{E_B}.

6 A Measurement of the Gluon Energy Spectrum in $b\bar{b}g$ Events

The observation of e^+e^- annihilation into final states containing three hadronic jets,[22] and their interpretation in terms of the process $e^+e^- \rightarrow q\overline{q}g$ (Ref. 23), provided the first direct evidence for the existence of the gluon, which is the gauge boson of the theory of the strong interactions, quantum chromodynamics

(QCD).[24] Following these initial observations, studies of the partition of energy among the three jets were performed at the DESY e^+e^- collider PETRA and the SLAC e^+e^- storage ring PEP. Comparison of the data with leading-order QCD predictions, and with a model incorporating the radiation of spin-0 (scalar) gluons, provided qualitative evidence[25] for the spin-1 (vector) nature of the gluon, which is a fundamental element of QCD. Similar studies have since been performed at the Z^0 resonance.[26]

In these previous studies the gluon jet was not explicitly tagged. Instead the jets were energy-ordered and the lowest-energy jet was assumed typically to be the gluon jet. If the gluon jet could be tagged event-by-event, more detailed studies of the structure of QCD could be performed. Due to advances in vertexing this is now possible using three-jet $b\overline{b}g$ events. The large mass and long lifetime, ~ 1.5 ps, of B hadrons lead to decay signatures which uniquely distinguish them from charm and light quark decays. With the high-precision VXD2 detector, we tag two jets containing B hadrons in three-jet events by counting the number of tracks in the jets that are inconsistent with coming from the primary IP. Thus, we tag the gluon jet on an event-by-event basis. A similar technique has been used recently by the OPAL Collaboration, to investigate differences between quark and gluon jet properties.[27]

The fully corrected gluon scaled energy distribution is shown in Fig. 9, where it is compared with QCD predictions calculated using JETSET 7.4. We evaluated the $O(\alpha_s)$, $O(\alpha_s^2)$, and parton shower (PS) predictions. The $O(\alpha_s)$ and the $O(\alpha_s^2)$ predictions describe the data well except in the region $0.2 < z < 0.4$. The PS prediction describes the data well across the full z range, suggesting that multiple orders of parton radiation are required for a good description.

The chromomagnetic moment of the bottom quark is induced at the one-loop level in QCD and is of the order α_s/π. One can also write down an *ad hoc* Lagrangian[28] with a $b\overline{b}g$ coupling modified via anomalous chromoelectric and chromomagnetic moments:

$$\mathcal{L}^{b\overline{b}g} = g_s \overline{b} T_a \{\gamma_\mu + \frac{i\sigma_{\mu\nu}k^\nu}{2m_b}(\kappa - i\tilde{\kappa}\gamma_5)\} b G_a^\mu, \tag{7}$$

where g_s is the strong charge, T_a is the $SU(3)_c$ generators, m_b is the bottom quark mass, k is the outgoing gluon momentum, and κ and $\tilde{\kappa}$ parameterize the anomalous chromomagnetic and chromoelectric moments, respectively, which might arise from physics beyond the Standard Model. The effect of the former on three-jet

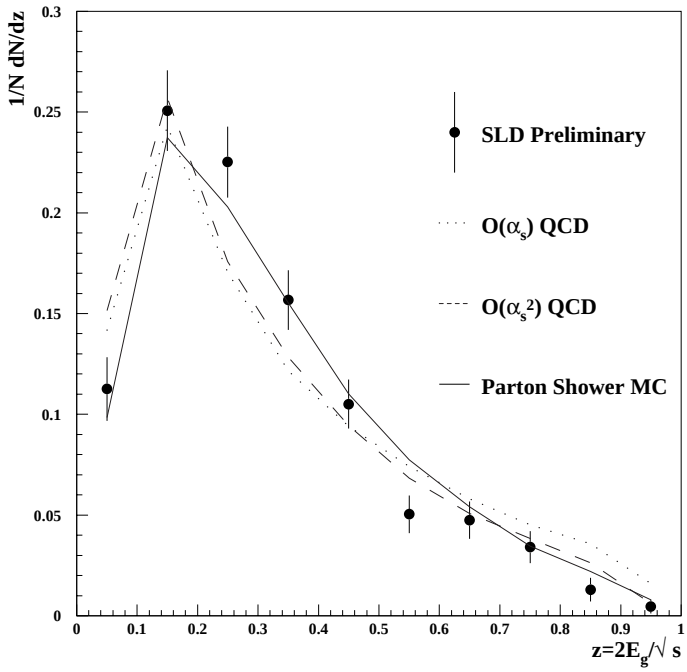

Figure 9: A comparison of the fully corrected gluon energy distribution with pertinent QCD predictions.

observables has been calculated recently.[28,29] The latter is CP-violating, and in this analysis we have not attempted to discriminate between the b and $\overline{b}$ jets and are hence insensitive to non-zero values of $\tilde{\kappa}$. As shown in Fig. 10, non-zero values of κ would harden the gluon energy distribution in $b\overline{b}g$ events.

Assuming the MC parton shower predictions approximate higher-order QCD, we fit for the value of an anomalous chromomagnetic moment, κ, and measured

$$\kappa = -0.030^{+0.061}_{-0.062}(stat.)^{+0.012}_{-0.003}(syst.) \quad (Preliminary).$$

We set 95% confidence-level limits of

$$-0.15 < \kappa < 0.09 \quad (Preliminary).$$

Further discussion of this analysis may be found in Ref. 30.

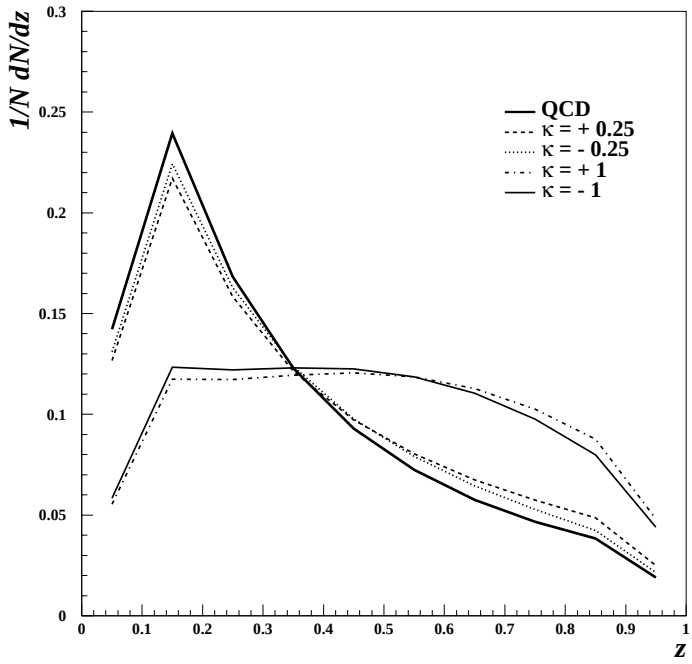

Figure 10: The effects of a non-zero chromomagnetic moment κ on the energy spectrum of the gluon.

7 Measurements of the B^+ and B^0 Lifetimes

The spectator model predicts that the lifetime of a heavy hadron depends upon the properties of the constituent weakly decaying heavy quark Q and is independent of the remaining, or spectator, quarks in the hadron. This model fails for the charm hadron system where the lifetime hierarchy $\tau_{D^+} \sim 2\tau_{D_s^+} \sim 2.5\tau_{D^0} \sim 5\tau_{\Lambda_c^+}$ is observed. Since corrections to the spectator model are predicted to scale with $1/m_Q^2$, the B meson lifetimes are expected to differ by less than 10%.[31] Hence, a measurement of the B^+ and B^0 lifetimes provides a test of this prediction. In addition, the specific B meson lifetimes are needed for precise determinations of the element V_{cb} of the CKM matrix.

Most measurements of the B^+ and B^0 lifetimes[32] are based on samples of semileptonic decays in which the lepton is identified and a $D^{(*)}$ meson is fully reconstructed. Fully exclusive[33] or inclusive[34] techniques have also been used.

Except for the inclusive technique, the efficiencies are typically small. Here, we present two complementary analyses that exploit the excellent three-dimensional vertexing capabilities of SLD to reconstruct the B meson decay length and measure its charge directly with high efficiency. The first analysis uses topological vertexing to identify B hadron decay vertices. The decay length is measured using the reconstructed vertex location while the B hadron charge is determined from the total charge of the tracks associated with the vertex. This inclusive technique is very efficient since most B decay modes are used. The second analysis identifies the B hadron charge by reconstructing the charged track topology of both B and cascade D vertices in semileptonic B decays. This technique has lower efficiency but benefits from an increased charge reconstruction purity. In contrast to previous measurements based on semileptonic decays, these two analyses do not rely on assumptions concerning the B^+ and B^0 content of $\overline{D^0}Xl^+\nu$ and $D^{(*)-}Xl^+\nu$ samples; rather, they only rely on the simple difference of total charge between B^+ and B^0 decays.

7.1 "Topological Vertexing" Analysis

The analysis is performed on the 1993–95 data sample of 150,000 hadronic Z^0 decays collected with the original vertex detector VXD2, together with 50,000 hadronic Z^0 decays collected using the upgraded vertex detector VXD3 in 1996. The inclusive topological vertexing technique is used to identify $\sim$ 21,000 B hadron vertices produced in hadronic Z^0 decays with high efficiency. The decay length is measured using the reconstructed vertex location while the B hadron charge is determined from the total charge of the tracks associated with the vertex.

Figure 11 shows a comparison of the reconstructed charge between data and Monte Carlo for (a) VXD2 and (b) VXD3. At this stage the charged sample consists of 8,676 (4,165) vertices with vertex charge equal to $\pm$1, 2, or 3, while the neutral sample consists of 5,197 (2,745) vertices with charge equal to 0 for VXD2 (VXD3) data. Monte Carlo studies indicate that for VXD2 (VXD3) the charged sample is 97.0% (97.6%) pure in B hadrons consisting of 52.4% (55.1%) $B^{\pm}$, 33.8% (32.0%) B^0, 9.1% (8.6%) B_s^0, and 4.7% (4.3%) B baryons. Similarly, the neutral sample is 97.9% (98.2%) pure in B hadrons consisting of 26.8% (24.1%) $B^{\pm}$, 52.4% (54.1%) B^0, 14.2% (15.0%) B_s^0, and 6.6% (6.8%) B baryons.

The lifetime measurement relies on the ability to separate B^+ and B^0 decays by making use of the vertex charge. The charge reconstruction in Fig. 11 shows good agreement between data and MC. A further check is made using the polarized forward-backward asymmetry. Using negative (positive) vertex charge, with vertices weighted by the M_{P_T}-dependent analyzing power,* to tag the b ($\overline{b}$) quark flavor, the resulting forward-backward asymmetry is sensitive to the accuracy of the vertex charge reconstruction. Good agreement between data and MC can be seen in Fig. 12 for all data-taking periods, indicating that the MC adequately reproduces the charge reconstruction purity of the data.

Information from the initial state tag (see Sec. 4) is used to enhance the charged sample purity by giving a higher (lower) weight to the B^+ hypothesis if the vertex charge agrees (disagrees) with the $b/\overline{b}$ tag. Including the initial state tag information enhances the statistical power of the analysis by $\sim 20\%$.

The B^+ and B^0 lifetimes are extracted using a simultaneous binned χ^2 fit to the decay length distributions of the B vertices in the charged and neutral samples. Figure 13 shows the reconstructed decay length for data and best fit MC for the two data sets and the charged and neutral samples. The two-parameter fit to the 1993–95 data yields lifetimes of $\tau_{B^+} = 1.724 \pm 0.051$ ps and $\tau_{B^0} = 1.567 \pm 0.055$ ps, with a ratio of $\tau_{B^+}/\tau_{B^0} = 1.100^{+0.068}_{-0.064}$ and a combined χ^2/d.o.f. $= 87.8/76$. The fit to the smaller 1996 VXD3 data sample yields lifetimes of $\tau_{B^+} = 1.654 \pm 0.066$ ps and $\tau_{B^0} = 1.603 \pm 0.069$ ps, with a ratio of $\tau_{B^+}/\tau_{B^0} = 1.032^{+0.081}_{-0.075}$ and a χ^2/d.o.f. $= 79.3/76$.

The combined 1993–95 and 1996 measurements yield the following preliminary result:

$$\begin{aligned}
\tau_{B^+} &= 1.698 \pm 0.040(stat.) \pm 0.046(syst.) \text{ ps}, \\
\tau_{B^0} &= 1.581 \pm 0.043(stat.) \pm 0.061(syst.) \text{ ps}, \\
\frac{\tau_{B^+}}{\tau_{B^0}} &= 1.072 \pm {}^{0.052}_{0.049}(stat.) \pm 0.038(syst.).
\end{aligned}$$

These results are consistent with the expectation that the B^+ and B^0 lifetimes are nearly equal and may indicate a slight deviation from equality. These measurements have a statistical accuracy among the best of the current measurements.[35] Further details of this analysis may be found in Ref. 36.

*The *analyzing power* is defined to be $\frac{P_{correct}-P_{incorrect}}{P_{correct}+P_{incorrect}} = (2|P_{correct}| - 1)$.

7.2 "Lepton + $D^{(*)}$" Semileptonic Analysis

The B^+ and B^0 lifetime measurements presented here use the 150,000 hadronic Z^0 decays collected between 1993 and 1995. The goal of this analysis is to reconstruct the charged track topology of semileptonic B decays. The algorithm reconstructs both B and cascade D vertices. The B vertex contains the lepton and at most one other track, and the D vertex contains two, three, or four tracks. This technique does not use the charge correlation between the lepton and the D vertex but simply determines the total charge of the B meson from the sum of charges in the B and D vertices. The final charge assignment purity will be somewhat diluted, however, due to the fraction of decays of the type $B^+ \to \bar{D}^{**0} l^+ \nu$, which can yield two slow transition pions at the B vertex.

Semileptonic B decay candidates are reconstructed using the same procedure as that discussed in Sec. 6. This technique reconstructs 634 charged candidates and 584 neutral candidates. From MC studies, the flavor contents are 66.9% B_u^+, 22.5% B_d^0, 5.7% B_s^0, and 2.4% B baryons for the charged sample, and 19.6% B_u^+, 60.8% B_d^0, 14.0% B_s^0, and 4.7% B baryons for the neutral sample.

Once again, the B^+ and B^0 lifetimes are extracted from the decay length distributions of the B vertices in the charged and neutral samples using a binned χ^2 fit (Fig. 14). These distributions are fitted simultaneously to determine the B^+ and B^0 lifetimes. The semileptonic analysis yields the following results:

$$\tau_{B^+} = 1.61^{+0.13}_{-0.12}(stat.) \pm 0.07(syst.) \text{ ps},$$

$$\tau_{B^0} = 1.56^{+0.14}_{-0.13}(stat.) \pm 0.10(syst.) \text{ ps},$$

with a ratio of:

$$\frac{\tau_{B^+}}{\tau_{B^0}} = 1.03^{+0.16}_{-0.14}(stat) \pm 0.09(syst).$$

These results are in good agreement with the current world averages and with the expectation that B^+ and B^0 lifetimes are nearly equal. Further discussion of this analysis may be found in Ref. 37.

8 Particle Production in Heavy- and Light-Quark Events

The production of final state hadrons from primary hard partons, e.g., the quark and antiquark in $e^+e^- \to Z^0 \to q\bar{q}$, is currently believed to proceed in three stages.

The first stage involves the radiation of gluons from the primary quark and antiquark, which in turn radiate gluons or split into $q\bar{q}$ pairs until their virtuality approaches the hadron mass scale. Such a "parton shower" is calculable in perturbative QCD, for example, in the Modified Leading Logarithm Approximation (MLLA).[38]

The second stage, in which these partons turn into "primary" hadrons, is not understood quantitatively, although several MC hadronization models exist.

The third stage, in which unstable primary hadrons decay into final state hadrons, complicates the interpretation of inclusive measurements. It is desirable to remove the effects of these decays when comparing with the predictions of hadronization models. Additional complications arise in jets initiated by heavy (c or b) quarks in which the leading heavy hadrons carry a large fraction of the beam energy, restricting that available to other primary particles, and then decay into a number of secondary particles. It is thus also desirable to restrict measurements to events with light primary flavors.

In this analysis we examine $\pi^{\pm}$, $K^{\pm}$, K^0, $K^{*0}/\bar{K}^{*0}$, ϕ, p/$\bar{\rm p}$, and $\Lambda^0/\bar{\Lambda}^0$ production in hadronic Z^0 decays. We use the CRID to identify the charged hadrons, as well as the neutral $K^{*0}/\bar{K}^{*0}$ and ϕ. The other neutral particles are identified using kinematic reconstruction. We measure differential cross sections in an inclusive sample of hadronic events of all flavors, and also in high-purity samples of light- ($Z^0 \to u\bar{u}, d\bar{d}, s\bar{s}$) and b-flavor ($Z^0 \to b\bar{b}$) events. From these three samples, tagged using the impact parameter technique, we extract corrected differential cross sections in light-, b-, and c-flavor ($Z^0 \to c\bar{c}$) events. The unfolded differential cross sections for the light-flavor events are free from effects of heavy quark production and decay. We use these measurements to test the predictions of various fragmentation models.

Figure 15 shows the corrected differential cross sections as a function of scaled momentum in $Z^0 \to u\bar{u}, d\bar{d}, s\bar{s}$ decays. These unfolded momentum distributions are free of the effects of heavy quark production and decay. The production of charged kaons is consistent with that of neutral kaons. The production ratios K:π and Λ^0:p show similar momentum dependence.

In Fig. 16 we show the ratios of production in b-flavor to light-flavor events for the seven species. The systematic errors on the particle identification largely cancel in the ratio, and the errors are predominantly statistical. There is higher production of charged pions in b-flavor at low momentum, with an approximately

constant ratio for $0.02 < x_p < 0.07$. The production of both charged and neutral kaons is approximately equal in the two samples at $x_p \leq 0.02$, but the relative production in b-flavor events then increases with x_p, peaking at $x_p \approx 0.07$. There is approximately equal production of baryons in b-flavor and light-flavor events below $x_p = 0.10$. For $x_p > 0.10$, production of pions, kaons, and protons falls off faster in b-flavor events. These features are consistent with expectations based on the known production and decay characteristics of heavy hadrons. Also shown in Fig. 16 are the predictions of the JETSET 7.4 and HERWIG 5.7 event generators,[39,40] both of which reproduce these features qualitatively. The exact values of these ratios depend on details of the B and D hadron production energy spectrum, as well as theory, and so provide information complementary to that in Fig. 15. Further discussion of this analysis may be found in Ref. 41.

9 An Inclusive Search for Enhanced $b \to sg$

It has been suggested[42] that there are several discrepancies between data and theory that may be resolved if the branching ratio for $b \to sg$ transitions is far in excess to that predicted by the Standard Model. The measured B semileptonic branching ratio $\mathrm{B}(b \to Xl\nu)$ is $\sim 11\%$ (Ref. 43), and the charmed multiplicity n_c, i.e., the number of charmed (and $\bar{c}$) quarks produced per b-quark decay is ~ 1.15–1.20 (Ref. 43). Neubert and Sachrajda[44] have shown that these quantities are correlated, so theory can accommodate the experimental value of $\mathrm{B}(b \to Xl\nu)$ only if $n_c = 1.3$. This disagreement could be resolved if the branching ratio $\mathrm{B}(b \to sg) \sim 10\%$, rather than the $\sim 0.2\%$ as currently estimated from Standard Model calculations. Current experimental limits on this process are very poor (approximately 10%) due to its poor experimental signature.

In the Standard Model, $b \to sg$ occurs through gluon penguins. Hypothetically, non-Standard Model TeV-scale physics that generates quark masses would also enhance the contribution from flavor-changing chromomagnetic dipole operators. This enhancement would then lead to enhanced flavor-changing branching ratios $\mathrm{B}(b \to sg)$ and $\mathrm{B}(b \to dg)$. The branching ratio $\mathrm{B}(b \to sg)$ could be enhanced by as much as a factor of ~ 50 without affecting the measured $\mathrm{B}(b \to s\gamma)$ values.

Experimentally, excess $b \to sg$ might be seen in charged kaon production. Figure 17 shows the predicted spectrum of $K^{\pm}$ in the rest frame of the B meson

for: (a) conventional $b \to c$ electroweak decays (thick solid line)[†], (b) excess kaon production with B($b \to sg$) $\sim$ 15% (dashed line), and (c) excess kaon production with B($b \to sg$) $\sim$ 10% (thin solid line). Clearly, over most of the momentum range the signal is masked by the large background contribution from the $b \to c$ transition. However, by restricting the study to those $K^{\pm}$ with momentum greater than 1.8 GeV/c, the signal-to-background approaches 1:1.

The procedure for the search is to: (i) reconstruct B candidates using topological vertexing (Sec. 3); (ii) identify charged kaons attached to these vertices using the CRID; and (iii) calculate the p_T of these kaons with respect to the B flight direction. We use p_T because it is Lorentz invariant and independent of the fragmentation function, and therefore has the same endpoint as p_{tot} in the rest frame of the B.

In order to reject $b \to c$ transitions, there must be no evidence for a tertiary vertex within the main topological vertex. This criterion is satisfied by calculating the probability that all tracks in the topological vertex come from a single decay point: When the fit probability is $> 5\%$, the event is classified as a "one-vertex" decay, or else it is classified as a "two-vertex" decay. MC studies indicate that true "one-vertex" decays (e.g., $B \to$ charmonium $+X$) are tagged correctly $\sim 79\%$ of the time. Furthermore, true "two-vertex" decays (e.g., hadronic $D + X$) are rejected $\sim 51\%$ of the time; this is only possible due to the high resolution of the VXD2 vertex detector.

Figure 18 shows that the kaon spectrum data are consistent with the MC predictions for the "two-vertex" (control) sample for $p_T > 1.8$ GeV/c. In the "one-vertex" sample, which is where we expect to see the $b \to sg$, the excess production in the 1993–95 data is 12.9 $\pm$ 5.9(stat.) $\pm$ 2.5(syst.) high-p_T events.

The largest systematic uncertainty comes from the modeling of the background from standard $b \to c$ decays, which is done using SLD's version of the CLEO B-decay model. The model indicates that the high p_T kaons come primarily (68%) from one source: D^0 decays. Since both the D^0 spectrum and the properties of D^0 decays have been well measured,[45] the uncertainty due to this source is fairly small (approximately 15%).

This measurement may be improved by requiring that the vertex does not contain an identified lepton. Preliminary studies indicate that the data and MC

[†]This is determined using the "SLD-tuned" JETSET generator with the CLEO B-decay model.[37]

predictions are consistent with each other in the "two-vertex" sample, and an excess persists in the data for the "one-vertex" sample. This excess is slightly more significant [15.9 $\pm$ 5.5(stat.)], but the systematics have not yet been evaluated.

10 Symmetry Tests in Polarized Z^0 Decays to $b\bar{b}g$

The forward-backward, polar-angle asymmetry in hadronic Z^0 decays to two jets has been investigated extensively at SLC and LEP to test the predictions of the electroweak theory of parity-violation in the $Z^0 q\bar{q}$ coupling. In particular, at SLC where the electron beam is highly polarized, the left-right-forward-backward asymmetry removes the dependence on the $Z^0 e^+ e^-$ coupling and is directly sensitive to the $Z^0 q\bar{q}$ coupling. The experimental results are found to be consistent with the theory to within experimental uncertainties of a few percent.[46] Hadronic Z^0 decays to three jets can be interpreted in terms of the fundamental process $Z^0 \to q\bar{q}g$ where one of the quarks has radiated a gluon. Given the success of the electroweak theory in predicting the two-jet polar-angle asymmetry, similar angular asymmetries can be measured in three-jet events to test Quantum Chromodynamics (QCD). The $Z^0 \to b\bar{b}g$ final state is particularly interesting since a high purity sample can be obtained with high efficiency due to the large mass and long lifetime of B hadrons.

In the three analyses discussed below, three-jet events were selected using the "Durham" jet algorithm.[47] A three-jet event was tagged as a $b\bar{b}$ event if at least one jet contained a vertex with $M_{vtx} > 1.5$ GeV/c^2. The highest energy jet was assumed to be a b- or $\bar{b}$-quark, and (where needed) the momentum-weighted jet charge was used to tag the jet's quark flavor. This procedure yielded 3,420 $b\bar{b}g$ events with a purity of 87%. Using these events, we performed the first experimental study of angular asymmetries in polarized Z^0 decays to $b\bar{b}g$. Further details may be found in Ref. 48.

10.1 A Study of Parity Violation in $Z^0 \to b\bar{b}g$ Events

Recently, Burrows and Osland have proposed new QCD tests in terms of the event orientation angles.[49] Integrating over scaled momenta and the azimuthal angle of the three-jet event plane with respect to the quark-electron plane, the polar angle

distribution of the thrust axis can be expressed as

$$\sigma(\cos\theta) \equiv \frac{d\sigma}{d\cos\theta} \propto (1 - P_{e^-} \cdot A_e)(1 + \alpha\cos^2\theta) + 2A_P(P_{e^-} - A_e)\cos\theta, \qquad (8)$$

where P_{e^-} is the electron beam polarization, and A_P is the parity violation parameter which is a product of the tree-level electroweak parameter A_b^{EW} corresponding to the $Zb\bar{b}$ vertex and a QCD factor A_b^{QCD} corresponding to the $b\bar{b}g$ vertex. Figure 19 shows the b-quark polar angle distributions for left- and right-handed electron beams.

By manipulating P_{e^-}, the left-right-forward-backward asymmetry, $\tilde{A}_{FB}$, is directly sensitive to the asymmetry parameter A_P,

$$\begin{aligned} \tilde{A}_{FB}(|\cos\theta|) &\equiv \frac{\sigma_L(|\cos\theta|) - \sigma_L(-|\cos\theta|) + \sigma_R(-|\cos\theta|) - \sigma_R(|\cos\theta|)}{\sigma_L(|\cos\theta|) + \sigma_L(-|\cos\theta|) + \sigma_R(-|\cos\theta|) + \sigma_R(|\cos\theta|)} \\ &= |P_e| A_P \frac{2|\cos\theta|}{1 + \cos^2\theta}. \end{aligned} \qquad (9)$$

Given the value of the electroweak parameter A_b^{EW}, measurement of the angular asymmetry parameters A_P in $Z^0 \to b\bar{b}g$ events allows one to test the QCD prediction for A_b^{QCD}.

After unfolding for efficiency and purity, a fit to the left-right-forward-backward asymmetry (Fig. 20) yields a value of the angular asymmetry parameter

$$A_P = 0.987 \pm 0.093(stat.) \pm 0.072(syst.) \quad (Preliminary).$$

Assuming the Standard Model expectation of $A_b^{EW} = 0.94$ for $\sin^2\theta_w = 0.23$, this yields a value of

$$A_b^{QCD} = 1.05 \pm 0.10(stat.) \pm 0.08(syst.) \quad (Preliminary).$$

This value is consistent with the $O(\alpha_s^2)$ QCD expectation of 0.93, calculated using the JETSET 7.4 event generator.[39]

10.2 A Search for T_N-Odd and CP-Violating Effects in $Z^0 \to b\bar{b}g$ Events

The differential cross section can also be expressed in terms of the polar angle ω of the vector $\bar{n}$ normal to the event plane with respect to the electron beam direction:

$$\frac{d\sigma}{d\cos\omega} \propto (1 - P_{e^-} \cdot A_e)(1 + \gamma\cos^2\omega) + 2A_T(P_{e^-} - A_e)\cos\omega. \qquad (10)$$

The second term is T-odd, and appears as a forward-backward asymmetry of the event-plane normal relative to the Z^0 polarization axis. At first order in perturbative QCD, the coefficient $A_T = 0$. The left-right-forward-backward asymmetry in $\cos\omega$ can also be defined by a similar double asymmetry as Eq. (9), and is directly proportional to the T-odd parameter A_T. The vector normal to the event plane can be defined in two ways: (1) the three jets are ordered according to their energies, and the two highest-energy jet momenta are used to define $\bar{n} = \vec{p_1} \times \vec{p_2}$; and (2) the quark and anti-quark momenta are used to define $\bar{n} = \vec{p_q} \times \vec{p_{\bar{q}}}$. The asymmetry term is CP-even in the first definition, and CP-odd in the second. The first definition does not require jet flavor identification, and the asymmetry has been studied for inclusive hadronic Z^0 decays.[50] The second definition requires tagging both quark- and antiquark-jets. In both cases, in the Standard Model the asymmetry vanishes identically at tree level, but higher-order processes yield non-zero contributions for $e^+e^- \to b\bar{b}g$. However, due to various cancellations, these contributions are found to be very small at the Z^0 resonance and yield values of the asymmetry parameter $|A_T| \lesssim 10^{-5}$ (Ref. 51). Measurement of the asymmetry in $\cos\omega$ is hence potentially sensitive to physics processes beyond the Standard Model.[52]

Figure 21 shows the left-right-forward-backward asymmetry of the $\cos\omega$ distribution for the two definitions: (a) $\vec{p_1} \times \vec{p_2}$, and (b) $\vec{p_b} \times \vec{p_{\bar{b}}}$. No asymmetry is apparent.

We performed maximum-likelihood fits to the $\cos\omega$ distributions to extract the parameters A_T^+, for the CP-even case, and A_T^-, for the CP-odd case.

We found

$$A_T^+ = -0.002 \pm 0.027 \quad (Preliminary),$$

$$A_T^- = -0.011 \pm 0.053 \quad (Preliminary),$$

where the error is statistical only. In both cases the T-odd contribution is consistent with zero within the statistical error and we calculate limits of

$$-0.056 < A_T^+ < 0.051 \quad at \quad 95\% \quad C.L. \quad (Preliminary),$$

$$-0.115 < A_T^- < 0.093 \quad at \quad 95\% \quad C.L. \quad (Preliminary).$$

11 $B^0 - \bar{B}^0$ Mixing

$B^0 - \overline{B^0}$ mixing occurs via a second-order weak interaction in complete analogy to the mixing observed in the $K^0 - \overline{K^0}$ system. The $|B^0\rangle$ flavor eigenstate is written in terms of the mass eigenstates $|B_1\rangle$ and $|B_2\rangle$, as $|B^0\rangle = (|B_1\rangle + |B_2\rangle)/\sqrt{2}$ and $|\overline{B^0}\rangle = (|B_1\rangle - |B_2\rangle)/\sqrt{2}$. Unlike the neutral kaon system, the difference between the B_1 and B_2 meson lifetimes is expected to be small. Hence, the probability that a meson created as a B^0 ($\overline{B^0}$) will decay as a B^0 ($\overline{B^0}$) after proper time t can be written as

$$P_u(t) = \frac{,}{2} e^{-,\,t} \left(1 + \cos \Delta m\, t\right) , \tag{11}$$

where Δm is the mass difference between the mass eigenstates, and , is the decay width for both states. The effects of CP violation are assumed to be small and are neglected. Similarly, the probability that the same initial state decays as its antiparticle is

$$P_m(t) = \frac{,}{2} e^{-,\,t} \left(1 - \cos \Delta m\, t\right) . \tag{12}$$

By measuring the oscillation frequency Δm, we are probing the related CKM matrix elements:

$$\Delta m_q = \frac{G_F^2}{6\pi^2} m_b m_t^2 F\left(\frac{m_t^2}{m_W^2}\right) B_{B_q} f_{B_q}^2 \eta_{QCD} \left|V_{tb}^* V_{tq}\right|^2 , \tag{13}$$

where $q = d,\ s$ for mixing in the B_d^0, B_s^0 systems. Thus, a measurement of Δm_d from $B_d^0 - \bar{B}_d^0$ mixing is sensitive to $|V_{td}|$, and a measurement of Δm_s from $B_s^0 - \bar{B}_s^0$ mixing is sensitive to $|V_{ts}|$. In both of these cases, however, the theoretical uncertainties are large. By combining B_d^0 and B_s^0 mixing measurements, one will be able to measure $|V_{ts}/V_{td}|^2$ with smaller theoretical uncertainty:

$$\Delta m_s / \Delta m_d = \left(\frac{f_{B_s}\sqrt{B_{B_s}}}{f_{B_d}\sqrt{B_{B_d}}}\right)^2 \frac{m_{B_s}}{m_{B_d}} \left|\frac{V_{ts}}{V_{td}}\right|^2 . \tag{14}$$

Current calculations of $(\frac{f_{B_s}\sqrt{B_{B_s}}}{f_{B_d}\sqrt{B_{B_d}}})^2$ indicate that it is approximately 1.15 ± 0.05 (Ref. 53).

In the next section, four measurements of Δm_d are summarized. Additional details may be found in Ref. 54. The section after that discusses projections for

SLD's sensitivity to $B_s^0 - \bar{B}_s^0$ mixing after the acquisition of 500,000 Z^0's with the new VXD3 vertex detector.

11.1 Four Measurements of $B_d^0 - \bar{B}_d^0$ Mixing

The outline of the procedure for all four $B_d^0 - \bar{B}_d^0$ mixing measurements is as follows:

1. Tag the *initial state* flavor of a hemisphere as b or $\bar{b}$ using the initial state tagging techniques discussed in Sec. 4 (i.e., the polarized forward-backward asymmetry combined with momentum-weighted jet charge).
2. Reconstruct the final state *decay point*.
3. Tag the *final state* flavor at the decay point.
4. Calculate the probability of an event having mixed from one flavor to the opposite.
5. Fit the fraction of decays tagged as mixed as a function of decay length to determine Δm_d.

The four methods used to determine Δm_d correspond to different techniques used to determine the final state flavor of the decay. Two analyses use the sign of a reconstructed lepton to tag the final state flavor, one uses the sign of reconstructed charged kaons, and the last uses a novel *charge dipole* technique. All four measurements use the 1993-1995 data set of 150,000 hadronic Z^0 decays.

The first lepton-tag analysis ("topological lepton") uses the same procedure as used in the semi-leptonic B lifetime analysis (Sec. 7.2): a lepton with $p_T > 0.4$ GeV/c is combined with a reconstructed D vertex. The sign of this lepton correctly identifies the flavor of the decay 85% of the time. The oscillation frequency measured in the sample of neutral B decays is:

$$\Delta m_d = 0.45 \pm 0.07(stat.) \pm 0.05(syst.)\ \mathrm{ps}^{-1} \quad (Preliminary).$$

The second lepton-tag analysis is more inclusive. A high-p_T lepton ($p_T > 0.8$ GeV/c) is intersected with tracks that have a high-impact parameter. Each intersection point is weighted by the angle of the track to the lepton and according to the probability that they originate from secondary decays. A weighted B vertex position is then calculated. The measured oscillation frequency is:

$$\Delta m_d = 0.52 \pm 0.07(stat.) \pm 0.04(syst.)\ \mathrm{ps}^{-1} \quad (Preliminary).$$

The third analysis uses the CRID to identify charged kaons that are attached to the topological vertex. This final state tag exploits the dominant $b \to c \to s$ transition. Thus, $K^-(K^+)$ tags $b(\bar{b})$ quarks at decay. The sign of the sum of identified kaons correctly identifies the flavor of B_d^0 decays 77% of the time. The measured oscillation frequency for this analysis is:

$$\Delta m_d = 0.580 \pm 0.066(stat.) \pm 0.075(syst.)\ \mathrm{ps}^{-1} \quad (Preliminary).$$

The final analysis uses a novel "charge dipole" tag, which exploits the $B \to D$ cascade charge structure to separate the final state $B^0/\overline{B^0}$ decay flavor. A sample enriched in B_d^0 decays is first selected by requiring that the total charge of the tracks associated with the vertex is equal to zero. The charge dipole δq of the vertex is defined as the relative displacement between the weighted mean location L_i of the positive tracks and of the negative tracks along the vertex axis taking each track at its point of closest approach to the vertex axis:

$$\delta q = (\sum^{+} w_i L_i)/(\sum^{+} w_i) - (\sum^{-} w_i L_i)/(\sum^{-} w_i),$$

where the first (second) term sums over all positive (negative) tracks in the vertex and the weight for track i is

$$w_i = \sin^2\theta_i/\sigma_{T_i},$$

where θ_i is the angle between track i and the vertex axis, and σ_{T_i} is the uncertainty in the impact parameter of track i to the vertex axis. Figure 22 shows the charge dipole distributions for the 1993–95 VXD2 data, along with the contributions from B_d^0 and $\bar{B}_d^0$ decays. The correct tag probability for this final state tag increases with the magnitude of δq, reaching a maximum of 84% in the tails.

The measured oscillation frequency for this inclusive analysis is:

$$\Delta m_d = 0.561 \pm 0.078(stat.) \pm 0.039(syst.)\ \mathrm{ps}^{-1} \quad (Preliminary).$$

A summary of all four mixed-fraction distributions is shown in Fig. 23. The weighted average of these four measurements, taking correlations into account, is

$$\Delta m_d = 0.526 \pm 0.043(stat.) \pm 0.031(syst.)\ \mathrm{ps}^{-1} \quad (Preliminary).$$

11.2 Prospects for Measuring $B_s^0 - \bar{B}_s^0$ Mixing at SLD

The mixing frequency for B_d^0 mixing, Δm_d, is now well measured; the August 1997 World Average is 0.472 ± 0.018 ps^{-1}. $B_s^0 - \bar{B}_s^0$ mixing has not yet been observed, but from LEP limits it is believed to be very fast: $\Delta m_s > 10.2$ ps^{-1} (95% C.L.). Thus, proper time (decay length) resolution is critical in order to observe this behavior. Specifically, in order to resolve a 1/4 oscillation with a frequency of 10 ps^{-1}, a proper time resolution of 0.15 ps is required, which translates into a decay length resolution of better than 300 μm.

At SLD, a study has been performed to estimate the "reach," or sensitivity, for observing $B_s^0 - \bar{B}_s^0$ mixing. In this study, three of the four final state tags used for the B_d^0 mixing analyses were examined: (i) "lepton + D," (ii) "inclusive lepton," and (iii) "charge dipole." In each case, the core decay length resolution is estimated to be better than 100 μm. For each case, the initial state tag was the same as that used for the B_d^0 analyses. The results of this study are shown in Fig. 24. Each analysis should have the statistical precision to quote a Δm_s lower limit as high as ~ 12 ps^{-1} (95% C.L.). By combining all three analyses, a Δm_s lower limit of ~ 16 ps^{-1} is achievable.

12 A Search for CP Violation in Inclusive B Decays

The "traditional" search for CP violation in B decays is to look at time-dependent asymmetries of the form:

$$A(t) = \frac{, (B^0(t) \to f) - , (B^{\bar{0}}(t) \to \bar{f})}{, (B^0(t) \to f) + , (B^{\bar{0}}(t) \to \bar{f})}, \tag{15}$$

where the final state f is a CP-eigenstate, i.e., $f = \bar{f}$. The "gold-plated" exclusive modes most often discussed are $f = \pi^+\pi^-$ for a measurement of the CKM Unitarity Triangle angle α, and $f = J/\psi K_s^0$ for a measurement of the angle β. These have clean experimental signature, but the branching ratios are low and the contribution to the asymmetries from penguin diagrams may be large.

Beneke *et al.*[55] proposed studying inclusive decay modes, as they predict that most of the hadronic uncertainties will cancel if many final states are summed over. Thus, a measurement of angle α may be made by examining inclusively

$B^0_d \to u\bar{u}d\bar{d}$, and a measurement of angle β may be made by examining inclusively $B^0_d \to c\bar{c}d\bar{d}$. It is predicted that the inclusive asymmetry could be sizable if non-Standard Model physics contributions exist. A dilution factor will be required to interpret this asymmetry in terms of CP violation, but this term should be calculable.

Beneke *et al.* have also calculated the all-inclusive asymmetry:

$$\begin{aligned} A(t) &= \frac{, (B^0(t) \to all) - , (\bar{B^0}(t) \to all)}{, (B^0(t) \to all) + , (\bar{B^0}(t) \to all)}, \\ &= a\left(\frac{\Delta m \tau_b}{2} \sin \Delta m t - \sin^2 \Delta m t\right), \end{aligned} \tag{16}$$

which measures the CP-violating parameter $a \simeq Im\left(\frac{\cdot 12}{M_{12}}\right)$. The Standard Model predicts that the asymmetry parameter $a = \mathrm{O}(10^{-3})$ for both B^0_d and B^0_s. As the B^0_s oscillation frequency Δm_s is known to be very large, and the fraction of B^0_s produced per primary b quark is low ($\sim 12\%$), a search was made for CP violation in B^0_d decays. In this analysis a measurement of a therefore corresponds to a measurement of the B^0_d asymmetry parameter a_d.

As the B^0_d oscillation frequency is large compared to its lifetime, no sensitivity was lost by studying the CP asymmetry in terms of decay length rather than proper time. Figure 25 indicates the MC predictions for the decay-length dependent asymmetry $A(d)$ for large input values of a_d. A large value of a_d would be clearly visible as a deviation of $A(d)$ from unity over most of the measured decay length range.

The analysis selected $b\bar{b}$ events in the 1993–96 data by requiring that at least one hemisphere contain a topological vertex with $M_{P_T} > 2.0$ GeV/c^2. Any hemisphere in this sample that contained a vertex, regardless of the vertex mass, was used for the analysis. No requirements were made for vertex charge, so two samples with different compositions were used. The neutral sample contained $\sim 50\%$ B^0_d's, and the charged vertex sample contained $\sim 35\%$ B^0_d's.

The initial state flavor of each hemisphere was tagged using a combination of the "standard" intial state tagging tools discussed in Sec. 4 (polarized forward-backward asymmetry + momentum-weighted jet charge) and (when available) additional information from the opposite hemisphere: high-p_T lepton charge, identified kaon charge, and vertex charge. Preliminary studies indicate that by using this additional information, the average effective tag purity was raised from 82% to 84% with 100% efficiency.

Figure 26 shows the experimental distribution $A(d)$. Each entry was weighted by the initial state tag analyzing power and by the B_d fraction in the sample. The binned asymmetry was fit to the functional form of Eq. (16) to extract a value for $a_d = -0.04 \pm 0.12(stat.) \pm 0.05(syst.)$, which results in a limit of

$$-0.29 < a_d < 0.22 \quad at \quad 95\% \quad C.L. \quad (Preliminary).$$

This represents the first measurement of the inclusive CP asymmetry for B_d^0 decays, and is consistent with expectations from the Standard Model.

13 Summary and Outlook

A series of measurements by the SLD Collaboration regarding various aspects of B production, mixing, and decay has been reviewed. Utilizing the combination of SLC's small and stable beam spots and SLD's precise CCD vertex detector, high purity samples of B hadrons were selected. When necessary, the initial state flavor of the heavy quark (i.e., b versus $\bar{b}$) was identified very efficiently by utilizing a combination of the forward-backward b-quark production asymmetry, which is greatly enhanced by the highly polarized electron beam, and the conventional momentum-weighted jet-charge technique. From these techniques, several new and precise measurements were made.

In June 1997 SLD started its most recent physics run. Slated to end in May of 1998, it is hoped that the current data set will be more than doubled. We anticipate that many of the above-mentioned results will improve, and that new and unique analysis results will be available in the future.

Acknowledgments

I wish to thank all SLD collaborators who have helped with the preparation for the talk and the proofreading of this paper. In particular, I would like to thank Stephane Willocq, Phil Burrows, Mark Convery, and Mourad Daoudi. I also wish to thank the authors of the SLD 1997 summer conference papers, from which I have borrowed heavily. Last but not least, I wish to thank the Summer Institute organizers for an enjoyable conference.

References

[1] See, for example, M. Woods, "The scanning Compton polarimeter for the SLD experiment," in *Proceedings of the 12th International Symposium on High-Energy Spin Physics* (Amsterdam, The Netherlands, September 1996), and references therein; R. Alley *et al.*, Nucl. Instrum. Methods A **365**, 1 (1995).

[2] "The SLD design report," SLAC Report 273, May 1984.

[3] G. D. Agnew *et al.*, in *Proceedings of the 26th International Conf. on High Energy Physics* (Dallas, Texas, 1992).

[4] K. Abe *et al.*, Nucl. Instrum. Methods A **386**, 46 (1997).

[5] K. Abe *et al.*, Nucl. Instrum. Methods A **343**, 74 (1996).

[6] D. J. Jackson, Nucl. Instrum. Methods A **388**, 247 (1997).

[7] B. Schumm, "Electroweak results from the SLD," SLAC-PUB-7697, November 1997.

[8] See, e.g., J. D. Bjorken, Phys. Rev. D **17**, 171 (1978).

[9] B. Mele and P. Nason, Phys. Lett. B **245**, 635 (1990); B. Mele and P. Nason, Nucl. Phys. B **361**, 626 (1991); G. Colangelo and P. Nason, Phys. Lett. B **285**, 167 (1992).

[10] Y. L. Dokshitzer, V. A. Khoze, and S. I. Troyan, Phys. Rev. D **53**, 89 (1996).

[11] E. Braaten, K. Cheung, and T. C. Yuan, Phys. Rev. D **48**, 5049 (1993); E. Braaten *et al.*, Phys. Rev. D **51**, 4819 (1995).

[12] M. G. Bowler, Z. Phys. C **11**, 169 (1981).

[13] C. Peterson *et al.*, Phys. Rev. D **27**, 105 (1983).

[14] B. Andersson *et al.*, Phys. Rep. **97**, 32 (1983).

[15] L. Randall and N. Rius, Nucl. Phys. B **441**, 167 (1995).

[16] The LEP Electroweak Working Group, D. Abbaneo *et al.*, LEPHF/96-01 (July 1996).

[17] ALEPH Collaboration, D. Buskulic *et al.*, Z. Phys. C **62**, 179 (1994);
DELPHI Collaboration, P. Abreu *et al.*, Z. Phys. C **66**, 323 (1995);
L3 Collaboration, O. Adeva *et al.*, Phys Lett. B **261**, 177 (1991);
OPAL Collaboration, P. D. Acton *et al.*, Z. Phys. C **60**, 199 (1993).

[18] See, for example, D. H. Saxon in *High energy electron-positron physics*, edited by A. Ali and P. Söding (World Scientific, 1988), p. 539.

[19] ALEPH Collaboration, D. Buskulic *et al.*, Phys. Lett. B **357**, 699 (1995).

[20] OPAL Collaboration, G. Alexander *et al.*, Phys. Lett. B **364**, 93 (1995).

[21] SLD Collaboration, K. Abe *et al.*, "A measurement of the B hadron energy distribution in Z^0 decays," July 1997.

[22] TASSO Collaboration, R. Brandelik *et al.*, Phys. Lett. B **86**, 243 (1979); Mark J Collaboration, D. P. Barber *et al.*, Phys. Rev. Lett. **43**, 830 (1979); PLUTO Collaboration, C. Berger *et al.*, Phys. Lett. B **86**, 418 (1979); JADE Collaboration, W. Bertal *et al.*, *ibid.* B **91**, 142 (1980).

[23] J. Ellis, M. K. Gaillard, and G. G. Ross, Nucl. Phys. B **111**, 253 (1976).

[24] H. Fritzsch, M. Gell-Mann, and H. Leutwyler, Phys. Lett. B **47**, 365 (1973); D. J. Gross and F. Wilczek, Phys. Rev. Lett. **30**, 1343 (1973); H. D. Politzer, *ibid.* **30**, 1346 (1973);

[25] TASSO Collaboration, R. Brandelik *et al.*, Phys. Lett. B **97**, 453 (1980); PLUTO Collaboration, C. Berger *et al.*, Phys. Lett. B **97**, 459 (1980); CELLO Collaboration, C. Berger *et al.*, Phys. Lett. B **110**, 329 (1982).

[26] L3 Collaboration, B. Adeve *et al.*, Phys. Lett. B **263** (1991) 551; OPAL Collaboration, Z. Phys. C **52**, 543 (1991); DELPHI Collaboration, P. Abreu *et al.*, Phys. Lett. B **274**, 498 (1992); SLD Collaboration, K. Abe *et al.*, Phys. Rev. D **55**, 2533 (1997).

[27] OPAL Collaboration, G. Alexander *et al.*, Phys. Lett. B **388**, 659 (1996).

[28] T. Rizzo, Phys. Rev. D **50**, 4478 (1994).

[29] T. Rizzo, private communication (1996).

[30] K. Abe *et al.*,"A preliminary study of the structure of $b\bar{b}g$ events using Z^0 decays," SLAC-PUB-7572, June 1997.

[31] See, for example, I. I. Bigi *et al.*, in *B Decays*, edited by S. Stone (World Scientific, New York, 1994), p. 132.

[32] D. Buskulic *et al.*, Z. Phys. C **71**, 31 (1996); P. Abreu *et al.*, Z. Phys. C **68**, 13 (1995); P. Abreu *et al.*, Report No. CERN-PPE/96-139 (1996); R. Akers *et al.*, Z. Phys. C **67**, 379 (1995); F. Abe *et al.*, Phys. Rev. Lett. **76**, 4462 (1996).

[33] F. Abe *et al.*, Phys. Rev. Lett. **72**, 3456 (1994).

[34] W. Adam *et al.*, Z. Phys. C **68**, 363 (1995).

[35] D. Buskulic *et al.*, Z. Phys. C **71**, 31 (1996); P. Abreu *et al.*, Z. Phys. C **68**, 13 (1995); P. Abreu *et al.*, Report No. CERN-PPE/96-139 (1996); W. Adam *et al.*, Z. Phys. C **68**, 363 (1995); R. Akers *et al.*, Z. Phys. C **67**, 379 (1995); F. Abe *et al.*, Phys. Rev. Lett. **76**, 4462 (1996); W. Adam *et al.*, Z. Phys. C **68**, 363 (1995); F. Abe *et al.*, Phys. Rev. Lett. **72**, 3456 (1994).

[36] K. Abe *et al.*, "Measurement of the B^+ and B^0 lifetimes from semileptonic and inclusive B decays," SLAC-PUB-7635, June 1997.

[37] K. Abe *et al.*, Phys. Rev. Lett. **75**, 3624 (1995).

[38] T. I. Azimov, Y. L. Dokshitzer, V. A. Khoze, and S. I. Troyan, Z. Phys. C **27**, 65 (1985).

[39] T. Sjöstrand, Computer Phys. Commun. **82**, 74 (1994).

[40] G. Marchesini and B. R. Webber, Nucl. Phys. B **310**, 453 (1988).

[41] K. Abe *et al.*,"Production of $\pi^{\pm}, K^{\pm}, K^0, K^{*0}, \phi,\ p$, and Λ^0 in hadronic Z^0 decays," SLAC-PUB-7571, June 1997.

[42] A. Kagan and J. Rathsman, "Hints for enhanced $b \to sg$ from charm and kaon counting," HEP-PH/9701300, January 1997.

[43] See, for example, J. Thaler, "Recent results from CLEO," in these proceedings.

[44] M. Neubert and C. T. Sachrajda, Nucl. Phys. B **483**, 339 (1997).

[45] L. Gibbons *et al.*, Phys. Rev. D **56**, 3783 (1997).

[46] K. Abe *et al.*, Phys. Rev. Lett. **74**, 2895 (1995) and references therein.

[47] S. Bethke *et al.*, Nucl. Phys. B **370**, 310 (1992).

[48] K. Abe *et al.*, "Symmetry tests in polarized Z^0 decays to $b\bar{b}g$," SLAC-PUB-7570, July 1997.

[49] P. N. Burrows and P. Osland, Phys. Lett. B **400**, 385 (1997).

[50] K. Abe *et al.*, Phys. Rev. Lett. **75**, 4173 (1996).

[51] A. Brandenburg, L. Dixon, and Y. Shadmi, Phys. Rev. D **53**, 1264 (1996).

[52] See, for example, C. D. Carone and H. Murayama, Phys. Rev. Lett. **74**, 3122 (1995).

[53] See, for example, L. K. Gibbons, "Status of weak quark mixing," UR-1494, April 1997, to appear in *Proceedings of ICHEP96* (Warsaw, Poland, July 1996), and references therein.

[54] K. Abe *et al.*, "Measurement of time-dependent $B^0_d - \bar{B}^0_d$ mixing using inclusive semileptonic decays," SLAC-PUB-7228, July 1996; K. Abe *et al.*, "Measurement of time-dependent $B^0_d - \bar{B}^0_d$ mixing using topology and charge-selected semileptonic decays," SLAC-PUB-7229, July 1996; K. Abe *et al.*, "Preliminary measurements of the time-dependence of $B^0_d - \bar{B}^0_d$ mixing with kaon and charge dipole tags," SLAC-PUB-7230, July 1996.

[55] M. Beneke, G. Buchalla, and I. Dunietz, Phys. Lett. B **393**, 132 (1997).

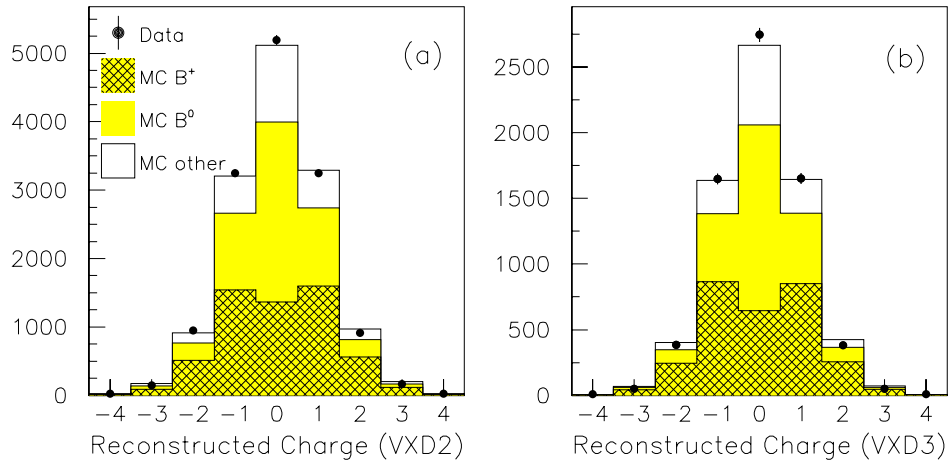

Figure 11: Reconstructed vertex charge for data (points) and Monte Carlo (histogram) for (a) 1993–95 data and (b) 1996 data.

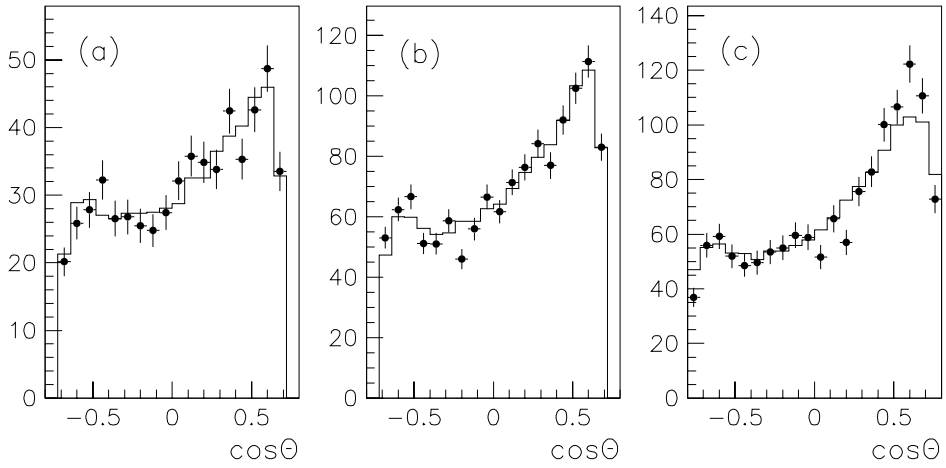

Figure 12: Distributions of cosθ signed by (P_e $\times$ vertex charge) for data (points) and Monte Carlo (histogram) for (a) 1993 (VXD2 and $|P_e| = 63\%$), (b) 1994–95 (VXD2 and $|P_e| = 77\%$), and (c) 1996 (VXD3 and $|P_e| = 76\%$).

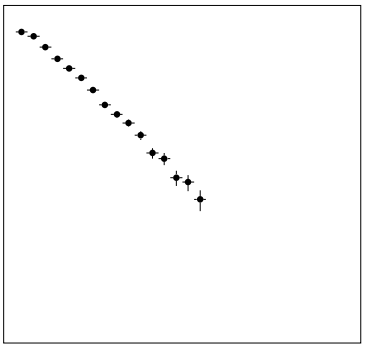

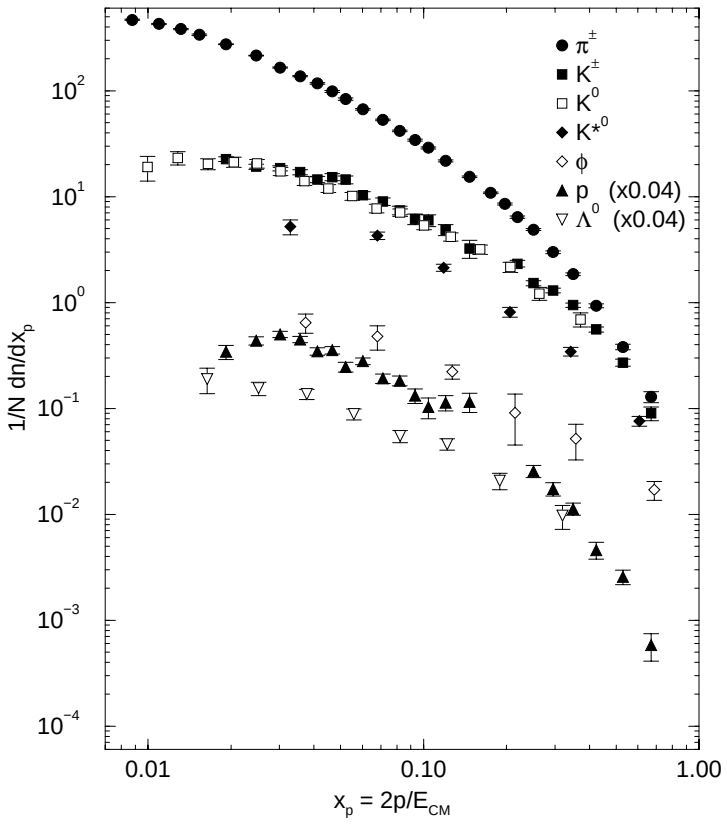

Figure 15: Identified particle production cross sections in $Z^0 \to u\bar{u}, d\bar{d}, s\bar{s}$ events (preliminary).

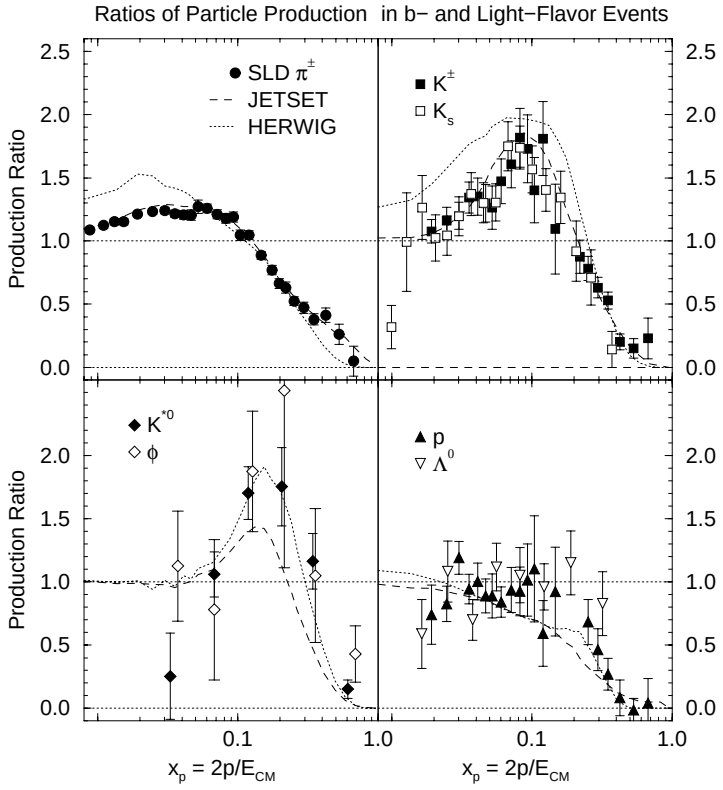

Figure 16: Ratios of production rates in b-flavor events to those in light-flavor events, along with the predictions of two fragmentation models. In the lower left plot, the dashed (dotted) line represents the JETSET prediction for K^{*0} (ϕ). In the right-hand plots, the predictions of a given model for the two particle types are very similar and have been averaged.

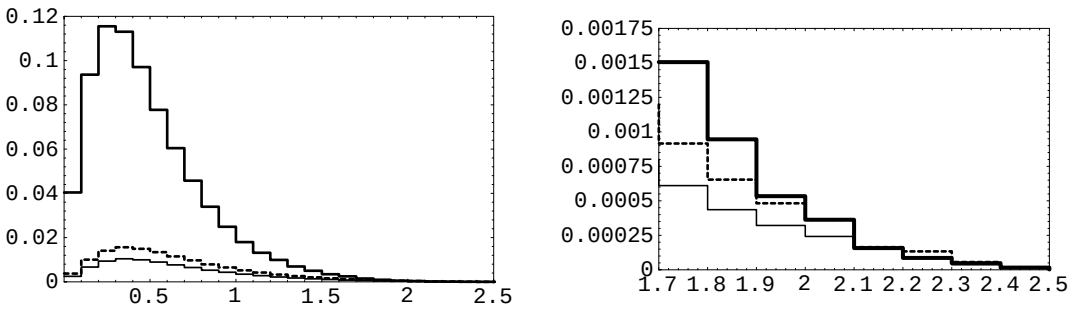

Figure 17: $\frac{1}{\sigma_{tot}}\frac{dn}{dp_{tot}}$ distributions for charged kaons from MC (see text).

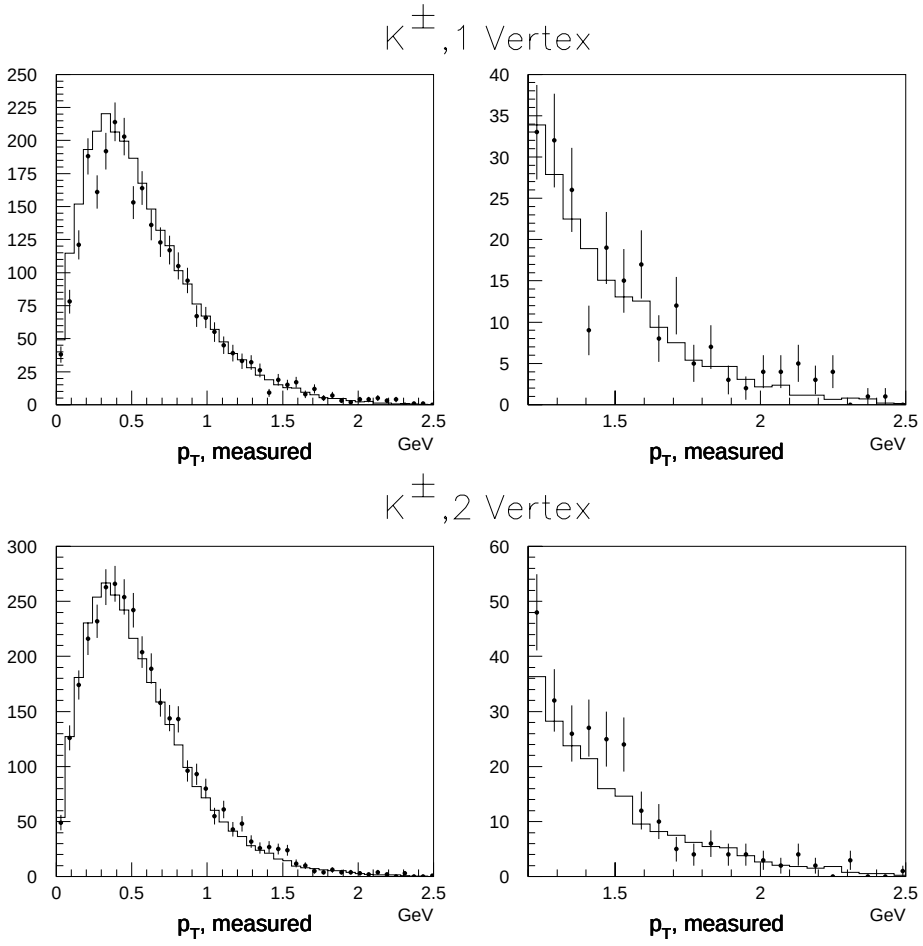

Figure 18: A comparison between the Data and MC predictions for the "one-vertex" sample (top), and for the "two-vertex" control sample (bottom). The right-most plots are magnifications of the high-p_T regions.

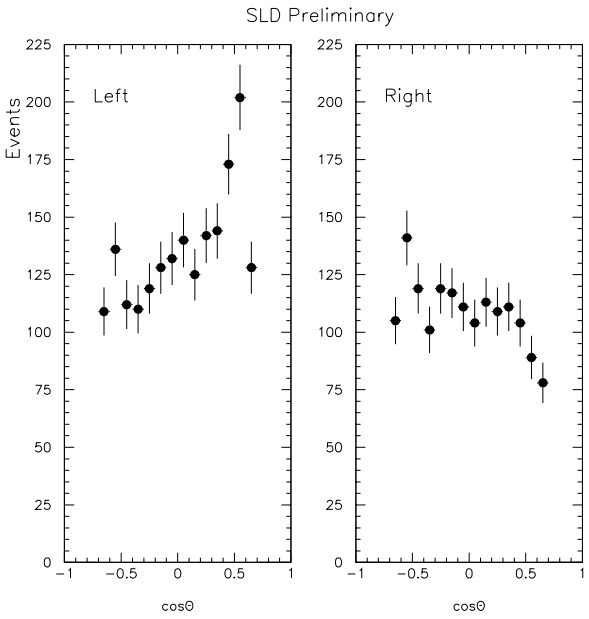

Figure 19: The polar angle distribution of the signed-thrust axis in $b\bar{b}g$ events with respect to the electron-beam direction for (a) left-handed and (b) right-handed electron beam.

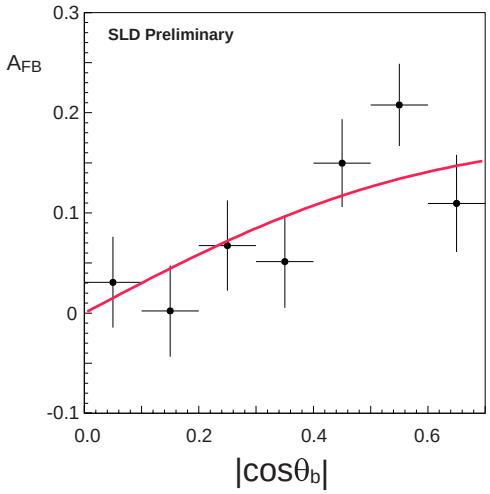

Figure 20: The fit to the left-right-forward-backward asymmetry distribution to determine the parity violating parameter A_P.

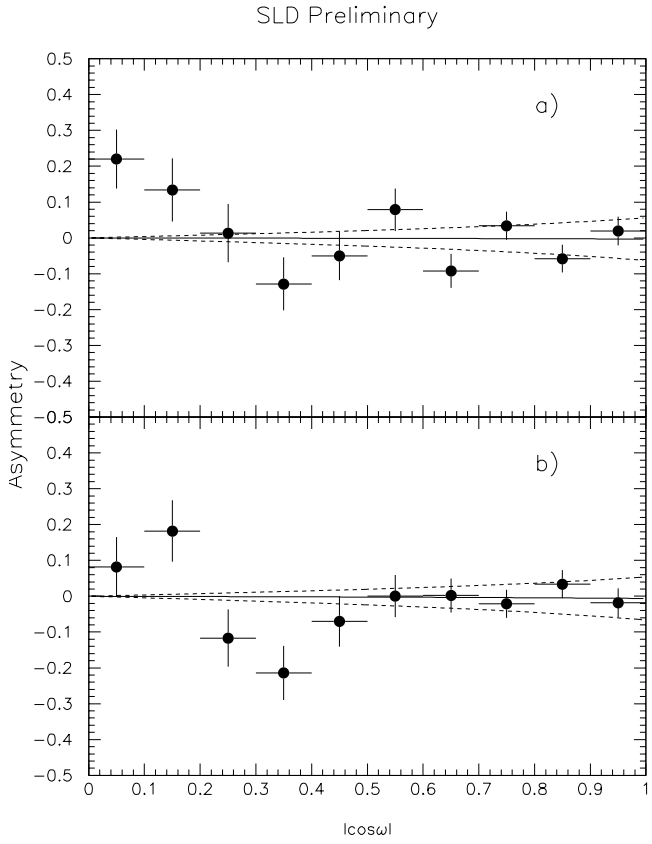

Figure 21: Left-right-forward-backward asymmetry in the polar-angle distribution of the vector normal to the event plane for the (a) CP-even case, and (b) CP-odd case. The solid curve is the best fit to the data sample, and the dashed curves correspond to the 95% C.L. limits.

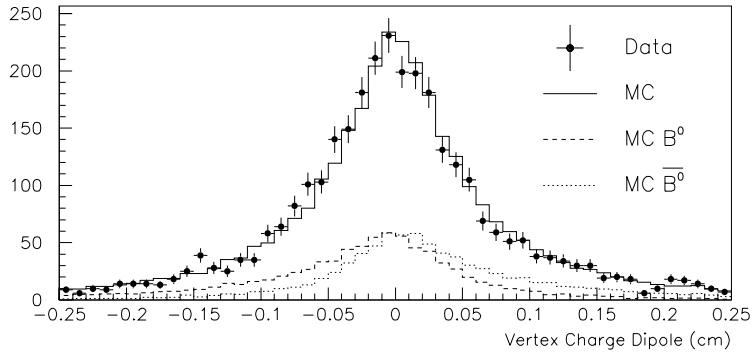

Figure 22: The vertex charge dipole distributions for the 1993–95 VXD2 data set. The solid circles indicate data, the dashed histogram indicates the B_d^0 contribution (from MC), and the dotted histogram indicates the $\bar{B}_d^0$ contribution. The solid histogram is the total of the B_d^0, $\bar{B}_d^0$, and non-signal contributions (e.g., $B^{\pm}$).

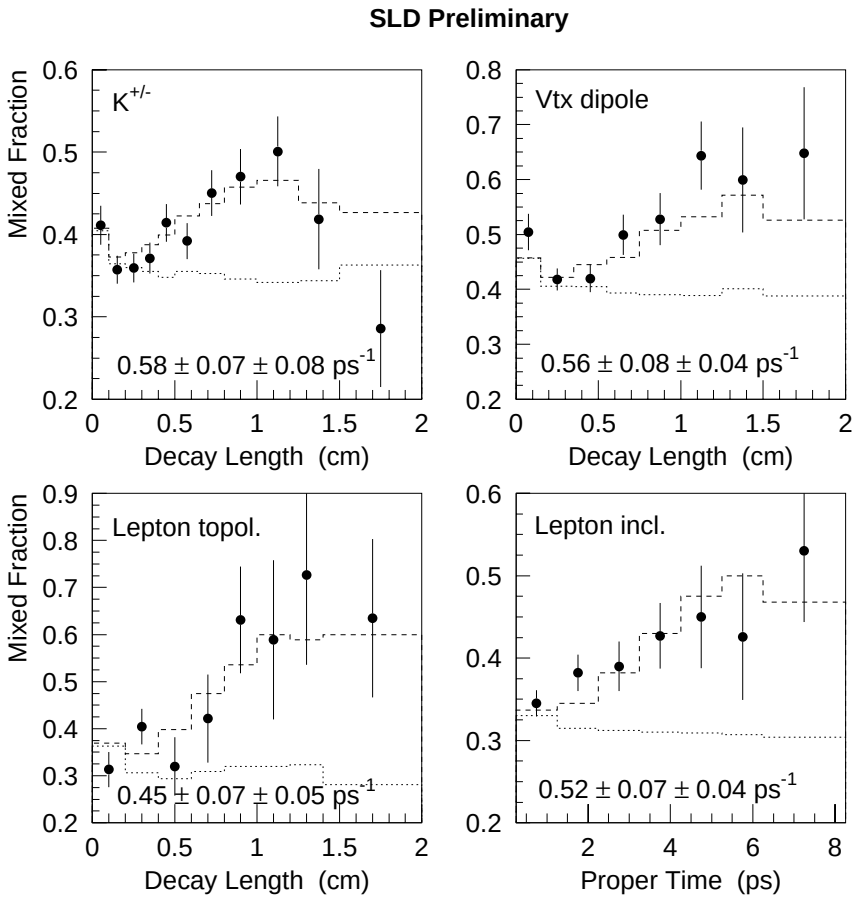

Figure 23: A summary of the four SLD B_d^0 mixing measurements. The points indicate the data, the dashed histograms indicate the best-fit mixing values from the MC, and the dotted histogram indicates the MC predictions for no B_d^0 mixing.

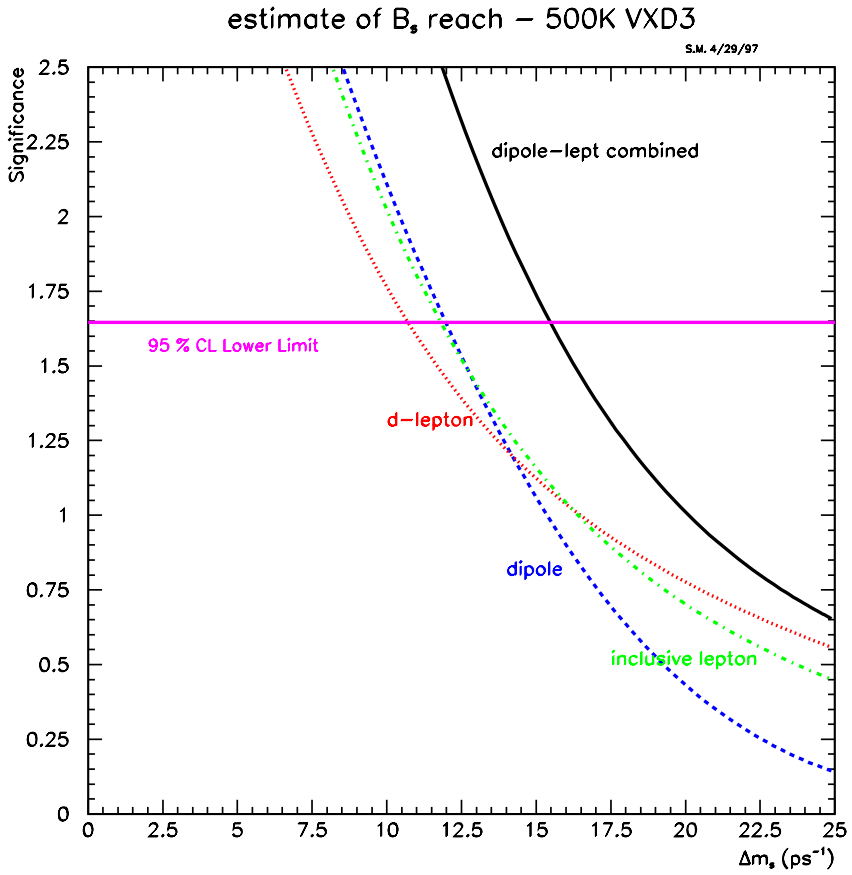

Figure 24: The estimated B_s^0 mixing reach for the SLD detector after acquiring 500,000 Z^0's with the new VXD3 vertex detector.

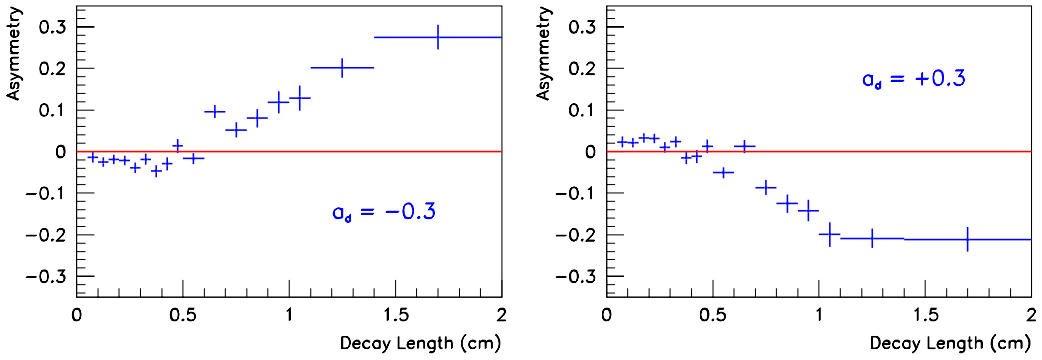

Figure 25: MC predictions for the decay-length dependent asymmetry $A(d)$ for input values of $a_d = \pm 0.30$.

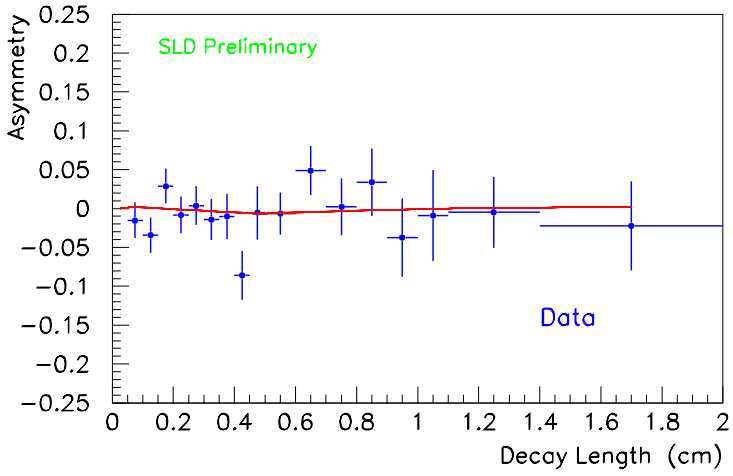

Figure 26: The measurement of $A(d)$ along with the fit to the function described in Eq. (16).